Structural interplay between strontium and calcium in α-CaHPO4 and β-SrHPO4

Structural Interplay between Strontium and Calcium in α-$CaHPO_4$ and β-$SrHPO_4$

Elisa Boanini[a,*], Massimo Gazzano[b], Katia Rubini[a], Paolo P. Mazzeo [c,d], Adriana Bigi[a]

a - Department of Chemistry "Giacomo Ciamician", Alma Mater Studiorum - University of Bologna, via Selmi 2, 40126 Bologna, Italy

b - ISOF-CNR, via Gobetti 101, 40129 Bologna, Italy

c - Dipartimento di Scienze Chimiche, della Vita e della Sostenibilità Ambientale, Università degli Studi di Parma, Viale delle Scienze, 17A, 43124 Parma, Italy.

d - Biopharmanet-TEC, Università degli Studi di Parma, Parco Area delle Scienze 27/A, 43124 Parma, Italy.

Corresponding author:

* Prof. Elisa Boanini: e-mail: elisa.boanini@unibo.it ; Tel: +39 051 2099548

Abstract

The ability of strontium ion to inhibit the abnormally high bone resorption, which occurs in pathologies characterized by loss of bone substance, has stimulated a number of research on strontium substituted/doped calcium phosphates. However, no information was available up to now on strontium substitution to calcium in the structure of α-$CaHPO_4$, monetite, in spite of the involvement of this phosphate in the composition of biomaterials for hard tissue substitution/repair and although it is isomorphous with α-$SrHPO_4$. Herein, we investigated the substitution of strontium to calcium in the structure of α-$CaHPO_4$, as well as the

replacement of calcium for strontium in the structure of a further polymorph of $SrHPO_4$, namely β-$SrHPO_4$. To this purpose, monetite at increasing degree of strontium substitution for calcium was synthesized by means of direct synthesis in aqueous solution, as well as through thermal treatment of strontium-substituted brushite; whereas the synthesis of β-$SrHPO_4$ was carried out at low temperature. The results of structural refinements, spectroscopic analysis and electron microscopy investigation indicate that the method of synthesis has a great influence on the range of strontium incorporation into α-$CaHPO_4$, which can reach 100 at%. The morphology of the synthesized materials is also remarkably dependent on composition. The analysis of the products synthesized at low temperature shows that the upper limit of possible substitution of calcium to strontium in the structure of β-$SrHPO_4$ is much more limited, just up to about 20 at%. Moreover, powder X-ray analysis of β-$SrHPO_4$ states that it crystallizes with a monoclinic cell in the space group $P2_1/c$.

Keywords: monetite; calcium phosphate; strontium phosphate; ionic substitution; crystal structure

1. INTRODUCTION

Strontium is of outmost interest among biologically relevant ions, as testified by the relevant amount of scientific researches on this ion, because of its positive role on bone metabolism. Most of body Sr^{2+} is found in bone, where it displays an heterogeneous distribution which implies higher concentrations in newly formed bone [1,2]. Its beneficial effect on bone remodeling occurs through two different actions: inhibition of osteoclast

formation and differentiation, and promotion of osteoblast proliferation and activity [3-7]. These characteristics make Sr ion an ideal candidate to counteract abnormal bone resorption occurring in pathologies such as osteoporosis. In fact, the use of strontium ranelate for the clinical treatment of osteoporosis has been approved in more than seventy countries [8]. The efficacy of strontium ranelate in stimulating osteogenesis and improving bone quality and strength has been supported by a number of studies [9-12].

The peculiar properties of strontium towards bone cells have been demonstrated to be maintained also when it is associated to calcium phosphates (CaPs) [13-19]. The studies on strontium substitution in CaPs are aimed to clarify the modifications induced by this ion on the chemistry, structure and morphology of these compounds and, at the same time, to verify their possible use as delivery systems of Sr [18-22]. CaPs are indeed the main inorganic components of bone and the studies on these materials provide useful information for a better understanding of the processes of biomineralization [23,24]. Strontium can replace calcium in the structure of hydroxyapatite in the whole range of composition provoking an enlargement of the unit cell, coherently with its bigger ionic radius [25-28]. A wide range of substitution, up to about 80 at %, has been reported also in β-tricalcium phosphate (β-TCP) [29-31]. On the other hand, the structures of the α form of tricalcium phosphate (α-TCP), as well as octacalcium phosphate (OCP) and brushite (DCPD), can support much smaller amount of strontium substitution for calcium [32-36], whereas the influence of strontium on monetite (DCPA), has not been explored up to now.

At room temperature the stable form of monetite, $CaHPO_4$, is the triclinic α form, space group P-1, which passes to P1 at low temperature [37-39]. The triclinic structure has been described as an assembly of $CaHPO_4$ chains linked by Ca–O bonds and three types of hydrogen bonds [40] (Figure 1), where the unit cell contains two pairs of PO_4 units. The

two crystallographically independent Ca atoms, Ca(1) and Ca(2), display seven and eight coordination, respectively, with similar mean Ca-O distances (Figure 1) [37]. Recently, a further polymorph, with an orthorhombic cell, space group $Ccm2_1$, has also been identified [41].

DCPA can be obtained by simple dehydration of DCPD, as well as through many other methods, including precipitation, hydrothermal synthesis, sol-gel, microwave assisted, ball-milling in the solid state [42-47]. Applications of DCPA span from food processing industry, to toothpaste, to orthopaedics [47,48]. Indeed, DCPA is utilized as a component of bone cements, and its good osteoconductive and osteoinductive properties are supported by a number of in vitro and in vivo studies [49-53].

In this study, we synthesized DCPA in the presence of increasing amounts of Sr^{2+}, with the aim to investigate the chemical, structural and morphological modifications induced by strontium substitution to calcium in the structure of DCPA. To this purpose, we utilized two different routes (Table S1): (i) direct synthesis in aqueous solution in the presence of increasing strontium concentrations; (ii) dehydration of strontium-substituted DCPD.

In addition to the α- form of $SrHPO_4$, which is isomorphous with monetite, two further polymorphs have been reported in the literature, namely β- and γ-$SrHPO_4$. Hexagonal shaped crystals of γ-$SrHPO_4$, with an orthorhombic cell, space group *Pbca* (No. 61) were obtained by hydrothermal synthesis by Taher et al. [54]. The same Authors reported that β-$SrHPO_4$ is isomorphous with the orthorhombic $BaHPO_4$, but the structure of this β form has not been resolved up to now. However, several methods of synthesis and different applications, including as drug carrier and as support for Pb^{2+} immobilization, have been reported for β-$SrHPO_4$ [55-57].

Herein, we solved the crystal structure of β-$SrHPO_4$ and explored its possibility to host calcium replacement to strontium.

2. MATERIALS AND METHODS

The conditions of synthesis utilized in this work are summarized in Table S1.

2.1 Direct Syntheses

Direct synthesis of $CaHPO_4$ (DCPA) was carried out by dropwise addition (2 ml/min) of 50 ml of 0.65 M $(NH_4)_2HPO_4$ solution to 50 ml of 1.08 M $Ca(NO_3)_2 \cdot 4H_2O$ solution at 90°C. The precipitate was maintained in contact with the reaction solution for 1 hour at 90°C under stirring, then centrifuged at 10,000 rpm for 10 minutes, washed twice with distilled water and dried at 37 °C. Sr-substituted DCPA samples were synthesized following the same procedure, but preparing the nitrate solution using the appropriate amounts of $Ca(NO_3)_2 \cdot 4H_2O$ and $Sr(NO_3)_2$: different compounds were prepared from solutions containing 0, 10, 20, 40, 60, 80 and 100 Sr atom%, calculated as ($[Sr^{2+} /(Ca^{2+} + Sr^{2+})] \cdot 100$). Total cation concentrations were kept 1.08 M. Samples were labelled DS-0, DS-10, DS-20, DS-40, DS-60, DS-80 and DS-100, respectively.

2.2 Syntheses through Thermal Treatment.

Synthesis of $CaHPO_4 \cdot 2H_2O$ (DCPD) was carried out using 150 ml of a phosphate solution containing 5 mmol of $Na_2HPO_4 \cdot 12H_2O$ and 5 mmol of $NaH_2PO_4 \cdot H_2O$, pH 4.90 adjusted with glacial CH_3COOH. The solution was heated at 37 °C and 50 mL of 0.2 M $Ca(CH_3COO)_2 \cdot H_2O$ was added dropwise over a period of about 20 minutes, under stirring. Afterwards the precipitate was stored in contact with the mother solution for 10 minutes, filtered, washed twice with bidistilled water and dried at 37°C. Sr-substituted DCPD samples were obtained similarly, but partially replacing $Ca(CH_3COO)_2 \cdot H_2O$ with

$Sr(CH_3COO)_2 \cdot ½H_2O$, to prepare solutions with different $[Sr^{2+} /(Ca^{2+} + Sr^{2+})] \cdot 100$ ratios, and a total cation concentration of 0.2 M: compounds were prepared from solutions containing 0, 10, 20, 40, and 60 Sr atom%. Samples were labelled DCPD-0, DCPD-10, DCPD-20, DCPD-40, and DCPD-60, respectively.

Thermal treatment of DCPD-0, DCPD-10, DCPD-20, DCPD-40, and DCPD-60 was performed at 300 °C for 30 min; afterwards samples were labelled TT-0, TT-10, TT-20, TT-40, and TT-60, respectively.

2.3 Syntheses at low temperature

For the synthesis of β-$SrHPO_4$, a flask containing 50 ml of 1.08 M $Sr(NO_3)_2$ was placed in an ice bath and the solution was allowed to cool to 5 °C, under stirring. Afterwards, dropwise addition of 50 ml of 0.65 M $(NH_4)_2HPO_4$ over a period of 20 minutes provoked the formation of a precipitate that was maintained in contact with the reaction solution for 1 hour at low temperature under stirring, then centrifuged at 10,000 rpm for 10 minutes, washed twice with distilled water and dried at 37 °C. Partial substitution of Sr with Ca was obtained following the same procedure, but preparing the nitrate solution using the appropriate amounts of $Ca(NO_3)_2 \cdot 4H_2O$ and $Sr(NO_3)_2$: different compounds were prepared from solutions containing 0, 60, 80 and 100 Sr atom%, calculated as $([Sr^{2+} /(Ca^{2+} + Sr^{2+})] \cdot 100)$. Total cation concentrations were kept 1.08 M. Samples were labelled β-0, β-60, β-80 and β-100, respectively.

2.4 Characterization

X-ray diffraction (XRD) investigation was performed using a PANalytical X'PertPro diffractometer in reflection geometry (Cu Kα radiation, λ = 0.15418 nm; X'Celerator detector). Samples were scanned in the 2θ range 5-60° by sampling 100s at each 0.1 step. A further data collection between 10 and 120° was carried out to apply profile fitting

procedure (step 0.033°/100s). HighScore Plus package version 4.9 by PANalytical was used for identification and Rietveld refinements. Strontium atoms were placed in the same position as calcium with the constraint that the total occupancy factors of Ca and Sr atoms at the same site must be equal to unit. Coherent lengths of crystalline domains were measured by Scherrer equation.

XRD data collection for structure solution from a powder sample of β-$SrHPO_4$ was performed in Bragg-Brentano geometry with CuKα radiation on a Rigaku SmartLab XE diffractometer equipped with a Hypix3000 2D Solid-State detector. Vertical variable slits program coupled with 2.5° soller slits were used to minimize peak asymmetry and intensity aberration at low angles. XRPD data were postprocessed and $CuK\alpha_2$ contribution was stripped using the proprietary Rigaku SmartLab Studio II software.

The details of the procedure carried out for structure solution are reported in Supplementary Information.

Ca and Sr contents in the solid products were analyzed by ion cromatography (Dionex ICS-90). Solid samples were previously dissolved in 0.1 M HCl.

For infrared absorption analysis in attenuated total reflection (FTIR-ATR) mode, samples were analyzed using a Bruker ALPHA FT-IR spectrometer equipped with a diamond unit, to collect 32 scans in the range 4000–400 cm^{-1} at a resolution of 4 cm^{-1}. Data analysis was operated with OPUS software.

Morphological investigation was performed using a Hitachi S-2400 scanning electron microscope (SEM) operating at 18 kV. Sputter-coating with gold was performed before examination. For TT-series samples, a Zeiss Leo-1530 high resolution scanning electron microscope operating at 1 kV (InLens detector) was used and no sample coating was performed.

Calorimetric measurements (DSC) were performed using a Perkin Elmer Pyris Diamond differential scanning calorimeter equipped with a model ULSP 90 intra-cooler Heating was carried out in aluminum open pan at 5 °C min^{-1} in the temperature range from 50 °C to 215 °C.

Thermogravimetric analysis (TGA) was carried out using a Perkin–Elmer TGA-7. Heating was performed in a platinum crucible in air flow (20 cm^3/min) at a rate of 10 °C/min up to 800 °C. The samples weights were in the range 5–10 mg.

3. RESULTS AND DISCUSSION

3.1 Sr-DCPA obtained by direct synthesis

The literature reports a variety of methods for the synthesis of monetite, α-$CaHPO_4$, and a higher Ca/P molar ratio than the stoichiometric value was sometimes successfully utilized [58, 59]. In particular, the conditions utilized in this work to synthesize monetite in the presence of increasing strontium concentration in solution allow to get products constituted by a single crystalline phase in the whole range of composition, as shown by the X-ray diffraction patterns reported in Figure 2a.

The comparison of the patterns of the products synthesized in the presence of Sr with that of pure DCPA, DS-0, puts into evidence a shift of the main diffraction peaks towards smaller angles on increasing the foreign ion concentration in solution (Figure 2b). The increasing enlargement of the interplanar distances suggests strontium incorporation into monetite structure. In agreement, chemical analysis of Sr content reported in Table 1 indicates a quantitative Sr incorporation into the solid phase. The X-ray pattern of DS-100 is that characteristic of α-$SrHPO_4$, which is isomorphous with α-$CaHPO_4$ [60].

Replacement of calcium with strontium, characterized by a greater scattering power, causes important variations in the diffraction intensities of several peaks (Figure 2b).

Table 1. Crystallographic and analytical data for DS samples.

	Cell parameters*						
Sample	a (Å)	b (Å)	c (Å)	alfa(°)	beta(°)	gamma(°)	V (Å^3)
DS-0	6.902	6.635	6.990	96.2	104.0	88.4	308.8
DS-10	6.919	6.643	7.004	96.1	104.1	88.5	310.5
DS-20	6.939	6.649	7.018	96.0	104.1	88.5	312.3
DS-40	7.030	6.695	7.099	95.2	104.8	88.8	321.8
DS-60	7.077	6.712	7.129	95.0	104.8	88.8	326.2
DS-80	7.138	6.752	7.186	94.7	104.9	88.9	333.5
DS-100	7.190	6.797	7.263	94.6	105.0	88.8	341.8
	Sr occupation factor*		Sr content (at%)		τ_{hkl} (nm)**		
Sample	site 1	site 2	Rietveld	Chemical	τ_{001}	$\tau_{0\text{-}11}$	$\tau_{1\text{-}20}$
DS-0	0.00	0.00	0	0	66	92	104
DS-10	0.05	0.03	4	6	58	62	63
DS-20	0.12	0.12	12	13	45	54	54
DS-40	0.30	0.46	38	35	34	45	23
DS-60	0.40	0.73	57	56	34	43	31
DS-80	0.72	0.84	78	79	39	40	48
DS-100	1.00	1.00	100	100	45	44	62

Notes: * estimated errors: a, b, c ± 0.002 Å, alfa, beta, gamma ±0.1°, V ± 0.1 Å^3, OF ±0.02.
** for $\tau_{1\text{-}20}$ relative to the couple 1 -2 0 / -1 -2 0 reflections. τ_{hkl} is the mean coherent length of the perfect crystalline domains along the orthogonal direction to the hkl plane

Structural refinements, which were performed with the Rietveld method [61], allowed to investigate the structural modifications induced by Sr on DCPA structure. Full pattern analyses of the samples synthesized in solution were carried out using the DCPA triclinic structure, space group P-1 (n. 2) and the atomic coordinates reported in the work by Catti et al. [37] as starting set. The results of the refinements reached convergence and good agreement indexes, as shown by the final plots reported in Figure 3a (DS-80) and in Figure

S1, and confirmed that all the samples are constituted of DCPA as the only crystalline phase.

The data reported in Table 1 show that the values of cell parameters increase on increasing Sr content, in agreement with the substitution of Ca ion (ionic radius: 0.112 nm) with the bigger Sr ion (ionic radius: 0.126 nm). In particular, the values of *a*, *b* and *c* increase linearly with the increase of Sr content from DCPA-0 to DCPA-100 (Figure 3b).

Sr content evaluated through structural refinements is in very good agreement with the analytical content and indicates that the ion incorporation in DCPA is less than the theoretical value at relatively low Sr concentrations in solution, but becomes almost quantitative on increasing Sr concentration.

The XRD patterns of the different samples show also variations of the broadness of the peaks as a function of Sr content. Measurement of FWHM (full width at half maximum) of some selected peaks was used to calculate the mean dimensions of the coherent length of the perfect crystalline domains (τ_{hkl}). The results (Table 1) indicate that these dimensions decrease up to a Sr content of about 50 at%, and then increase as Sr amount further increases up to 100 at%. A similar behavior was previously reported for Sr-substituted hydroxyapatite, where relatively low Sr replacement to calcium provoked a decrease of the coherent length of the perfect crystalline domains, whereas this parameter increased at relatively high strontium contents [25].

The values of the occupancy factors reported in Table 1 for samples at Sr contents less than 50 at% do not show a clear preference of Sr ion for one of the two crystallographycally independent metal sites, in agreement with their similar Ca-O mean distances [37]. However, samples at high Sr content exhibit a preferential occupancy for the metal site (2).

The ATR-IR spectrum of DS-0 displays intense absorption bands at 1127, 1059 and 991, due to P-O stretching, and at 886 cm^{-1} related to P-O(H) stretching. P-O-H in plane bending is responsible of the broad band between 1300 and 1450 cm^{-1}, whereas the absorption bands at about 559 and 523 cm^{-1} have been ascribed to O-P-O(H) bending mode [40, 62] (Figure 4a). The spectra recorded from samples at increasing Sr content show a shift of the absorption bands, most of which fall at increasing wavenumbers (Table S2), in agreement with the different Raman frequencies previously reported for α-$CaHPO_4$ and α-$SrHPO_4$ [63]. Moreover, the absorption bands in the spectrum of DS-100 exhibit a great relative intensity and a significantly greater sharpness than the other samples, in agreement with the high crystallinity of α- $SrHPO_4$.

The scanning electron microscopy images reported in Figure 4b show that pure monetite crystals are quite big and exhibit a layered morphology. The width of the crystals is about 5-10 μm and the thickness of the layers, which exhibit a smooth surface, is of 0.5-1 μm. The presence of strontium seems to promote the trend of the crystals to exfoliate: the layers become more numerous and thin on increasing Sr content. Simultaneously, crystals fragmentation increases and some rod-like crystals detach from the layers up to DS-100, which displays only rod-like crystals with mean dimension of 5x0.5 μm.

3.2 Sr-DCPA obtained by thermal treatment of Sr-DCPD

At variance with the results obtained on the incorporation of Sr into DCPA structure, we have recently demonstrated that strontium cannot substitute for calcium into the structure of DCPD in the whole range of composition [36]. The synthesis of brushite in the presence of increasing Sr concentration in solution yields a unique crystalline phase up to a strontium concentration in solution of 60 at%, and corresponds to a Sr content of about 38 at% in the

solid phase. It is known that DCPD loses its structural water molecules and converts into its anhydrous form, DCPA, by heat treatment at temperature higher than 180°C [64].

Figure 5a reports the DSC curves of the DCPD samples synthesized at increasing Sr content. The comparison clearly shows the shift of the endothermic peak corresponding to the thermal conversion of DCPD into DCPA towards lower temperature as a function of Sr content. The decrease of the temperature of the endothermic peak is accompanied by the decrease of the associated enthalpy variation (ΔH), in agreement with the increase of molecular weight due to Sr substitution for calcium (Table 2).

Table 2. Microcalorimetric data: DSC enthalpy variation and temperature of the endothermic transition from DCPD to DCPA; and TGA temperature of maximum weight loss speed corresponding to the removal of the two structural water molecules from the structure of DCPD.

	DSC		TGA
Sample	ΔH (J/g)	T (°C)	T (°C)
DCPD-0	412	192	217
DCPD-10	410	191	216
DCPD-20	405	189	215
DCPD-40	400	186	213
DCPD-60	378	178	207

The decrease of DCPD thermal stability on increasing Sr content is confirmed by the results of thermogravimetric analysis. The weight loss corresponding to the removal of the two structural water molecules from pure DCPD occurs between 100 and 300°C (Figure S2). The temperature of maximum weight loss speed gradually decreases from 217°C to 207°C (Table 2) on passing from DCPD-0 to DCPD-60.

The powder X-ray diffraction patterns of the products obtained through thermal treatment of the samples DCPD-0 to DCPD-60 confirm the presence of DCPA as unique crystalline phase (Figure 5b). The diffraction peaks present in the XRD patterns are generally less sharp (Table 3) than those of the corresponding samples obtained by direct synthesis, most likely because of the different method of preparation. Furthermore, the broadening of the peaks increases on increasing Sr content, suggesting a reduction of the dimensions of the coherent length of the perfect crystalline domains that is accompanied by a growing presence of amorphous material up to a value of about 30% in TT-60. Simultaneously, the presence of Sr provokes a shift of the main diffraction peaks of monetite towards lower angles, in agreement with a partial substitution of Sr for Ca into DCPA structure.

The results of the structural refinements show indeed an increase of the cell parameters on increasing Sr content (Table 3), with a similar trend to that observed for the samples obtained by direct synthesis.

Table 3. Crystallographic and analytical data for TT samples.

	Cell parameters*						
Sample	a (Å)	b (Å)	c (Å)	alfa(°)	beta(°)	gamma(°)	V (Å^3)
TT-0	6.914	6.644	7.000	96.2	104.0	88.4	310.25
TT-10	6.923	6.653	7.009	96.1	104.0	88.4	311.37
TT-20	6.932	6.653	7.022	96.0	104.1	88.4	312.40
TT-40	6.962	6.660	7.051	95.7	104.1	88.5	315.43
TT-60	7.020	6.688	7.096	95.4	104.6	88.6	321.03
	Occupation factor*		Sr content (at%)		X_c	τ_{hkl} (nm)**	
Sample	site 1	site 2	Rietveld	Chemical		τ_{001}	$\tau_{1\text{-}20}$
TT-0	0.00	0.00	0	0	96	30	311
TT-10	0.06	0.04	5	4	90	27	304
TT-20	0.04	0.10	7	7	83	27	27
TT-40	0.09	0.20	15	18	73	24	26
TT-60	0.34	0.38	36	34	71	17	21

Notes: * estimated errors: a, b, c ± 0.002 Å, alfa, beta, gamma ±0.1°, V ± 0.1 Å^3, OF ±0.02.

** for $\tau_{1\text{-}20}$ relative to the couple 1 -2 0 / -1 -2 0 reflections.

X_c: crystallinity evaluated by the ratio $A_{cry}*100/(A_{cry} + A_{amo})$ where A_{cry} and A_{amo} are the crystalline and amorphous portion of the X-ray integrated intensity

The ATR-IR spectrum of DCPA obtained by thermal treatment of DCPD (TT-0) is very similar to that of the sample obtained by direct synthesis (Figure S3). Moreover, the samples at increasing Sr content show similar shifts of the absorption bands as those observed for the products of the direct synthesis.

On the other hand, the morphologies of the TT samples are quite different from that of DS samples, and resemble those of the corresponding DCPD samples before heat treatment. In particular, the SEM image of TT-0 shows the presence of plate-like crystals, with a morphology very similar to that characteristic of DCPD-0 [36]. The images of samples at increasing strontium content confirm that the foreign ion promotes aggregation and layering of the crystals (Figure 5c).

3.3 β-$SrHPO_4$

We explored the possibility to substitute Ca for Sr into the structure of β-$SrHPO_4$. To this aim, we performed the same synthesis used for the α-form using a lower temperature, namely 5°C. In the absence of calcium ions, the synthesis yields β-$SrHPO_4$ as single crystalline phase (ICDD file 12-368), as shown by the XRD pattern reported in Figure 6a.

SEM image in Figure 6b shows that pure β-$SrHPO_4$, β-100 is constituted of clusters of thin flaky crystals. At variance with what found for the α-polymorph, this structure does not seem to tolerate relatively great amount of calcium ion incorporation. In fact, the products of synthesis performed in the presence of increasing calcium concentration in solution are constituted by a single crystalline phase just up to β-80 (Sr content: 72 at%), whereas greater Ca concentrations provoke the precipitation of secondary phases (Figure 10).

Calcium substitution for strontium in β-80 provokes a reduction of lattice parameters (*a*=10.197(3) Å, *b*=7.954(4) Å, *c*=9.303(3) Å, β=116.95(5)°, V=672.6(5) $Å^3$), and a remarkable morphological modification: it is constituted of a multitude of very small

crystals (mean dimension smaller than 100 nm) clustered together in aggregates of undefined shape, as shown in Figure 6b.

Interestingly, β-0, obtained through synthesis carried out in the same experimental conditions, but in the complete absence of Sr, is constituted of DCPD as unique crystalline phase (Figure 5a) confirming the inhibiting effect of calcium on β-$SrHPO_4$ structure. Figure 6b shows that β-0 exhibits the typical plate-like morphology of DCPD [64]. The ATR-IR spectra of both β-100 and β-80 exhibit a number of absorption bands in the regions characteristic of P-O and P-OH stretching and bending modes (Figure S4)

3.4 Structure of β-$SrHPO_4$

Since the structure of β-$SrHPO_4$ has not been solved up to now, the pattern of β-100 sample was indexed as a monoclinic cell with parameters *a*=10.239(2) Å, *b* =7.9992(17) Å, *c*=9.326 (2) Å, β = 116.770(4)°, V = 682.0(3) $Å^3$, space group $P2_1/c$ (n. 14), and atoms positioned from powder data, as detailed in Supplementary Information. A summary of crystal data is shown in Table S3, the final Rietveld plot is reported in Figure 7a and final atomic parameters are reported in Table S4 (file CSD2069793) The asymmetric unit consists of two Sr atoms and two hydrogen phosphate groups.

The structural arrangement, as seen along *c*-axis (Figure 7b) consists of alternate phosphate layers, P1a and P1b, parallel to b,c plane and spaced by Sr atoms. The environment of Sr1a is an irregular polyhedron with oxygen at height vertex at distances within 2.36÷2.86 Å. Sr1b is nine-coordinated at distances in the range 2.38-2.91 Å with geometry reminiscent of a pentagonal bipyramid in which the two apexes are substituted by a phosphate edge (Figure 7c,d). Coordination arrays of Sr polyhedral are parallel to b,c plane. The presence of nine-coordinated cationic site can justify the difficulty of calcium, which usually prefers smaller coordination numbers, to enter this structure in relevant amount.

Comparison with triclinic α-structure [60] and orthorhombic γ-structure [54] indicates that the unit cell volume of the β polymorph is twice as that of α- and a half of that of γ-structure. Moreover, in α-$SrHPO_4$ and γ-$SrHPO_4$ both Sr atoms are eight and nine coordinated, respectively, while β-structure presents both kinds of coordination. Thus, the structural details of β-$SrHPO_4$ can be described as intermediate between those of the triclinic and the orthorhombic structure.

4. CONCLUSIONS

In this work we determined the range of incorporation of strontium and calcium into α-$CaHPO_4$ and β-$SrHPO_4$ structures, respectively, and clarified structural details of the β-polymorph of $SrHPO_4$.

The results of the direct synthesis of α-$CaHPO_4$ samples indicate that strontium can replace calcium in the structure of DCPA in the whole range of composition up to the isomorph α-$SrHPO_4$. The substitution, which is roughly quantitative, provokes a linear expansion of the cell parameters in agreement with the larger ionic radius of strontium than calcium, and a shift of the phosphate infrared absorption bands. Solid solutions of intermediate composition exhibit a reduction of the length of the perfect crystalline domains and of the sharpness of the infrared absorption bands in comparison to those of the two end members. Moreover, strontium incorporation into DCPA structure implies a significant modification of the crystal morphology, from layered big crystals to much smaller rod-like crystals. At variance, the range of strontium substitution in monetite samples synthesized through thermal treatment of DCPD samples is dictated by the limited capacity of brushite structure to host strontium, which provokes a reduction of DCPD thermal stability. TT samples show

structural variations due to strontium incorporation similar to those observed for DS samples, whereas they maintain a morphology resembling that of DCPD and confirm the tendency to crystal aggregation induced by Sr incorporation.

Powder X-ray analysis of β-$SrHPO_4$ synthesized at low temperature provided detailed information on its crystal structure, which had not been resolved up to now. This polymorph crystallizes in a monoclinic cell, space group $P2_1/c$ (n. 14), where strontium occupies two independent sites. No calcium isomorph of this structure is known. In agreement, we found that calcium substitution to strontium into β-$SrHPO_4$ occurs just up to about 20%, whereas higher calcium concentrations in the synthesis solution provoke the precipitation of secondary phases.

The biological relevance of strontium ion, which is usefully employed in several pathologies of the skeletal system, is well known, as well as the increasing interest towards the applications of non apatitic calcium orthophosphates in the biomedical field. Thus, the results of this work not only provide new information on ionic substitution in (calcium) orthophosphates, but can also be usefully employed for the development of new biomaterials for orthopaedic applications.

Acknowledgment

The authors are grateful to the support of the University of Bologna. EB and AB acknowledge 'Departments of Excellence' program of the Italian Ministry for Education, University and Research (MIUR, 2018-2022). PPM acknowledges the COMP-HUB Initiative, funded by the 'Departments of Excellence' program of the Italian Ministry for Education, University and Research (MIUR, 2018-2022).

References

[1] P.J. Marie, P. Ammann, G. Boivin, C. Rey, Mechanisms of action and therapeutic potential of strontium in bone, Calcif. Tissue Int. 69 (2001) 121–129.

[2] G. Boivin, D. Farlay, M.T. Khebbab, X. Jaurand, P.D. Delmas, P.J. Meunier, In osteoporotic women treated with strontium ranelate, strontium is located in bone formed during treatment with a maintained degree of mineralization, Osteoporos. Int. 21 (2010) 667–677.

[3] M. Jimenez, C. Abradelo, J.S. Roman, L. Rojo, Bibliographic review on the state of the art of strontium and zinc based regenerative therapies. Recent developments and clinical applications, J. Mater. Chem. B 7 (2019) 1974–1985.

[4] M.D. Grynpas, E. Hamilton, R. Cheung, Y. Tsouderos, P. Deloffre, M. Hott, P.J. Marie, Strontium increases vertebral bone volume in rats at a low dose that does not induce detectable mineralization defect, Bone 18 (1996) 253–259.

[5] S. Peng, X.S. Liu, S. Huang, Z. Li, H. Pan, W. Zhen, K.D. Luk, X.E. Guo, W.W. Lu, The cross-talk between osteoclasts and osteoblasts in response to strontium treatment: involvement of osteoprotegerin, Bone 49 (2011) 1290–1298.

[6] F. Yang, D. Yang, J. Tu, Q. Zheng, L. Cai, L. Wang, Strontium enhances osteogenic differentiation of mesenchymal stem cells and in vivo bone formation by activating wnt/catenin signaling, Stem Cells 29 (2011) 981–991.

[7] M. Demirel, A.I. Kaya, Effect of strontium-containing compounds on bone grafts, J. Mater. Sci. 55 (2020) 6305–6329.

[8] Z. Wang, X. Wang, Y. Tian, J. Pei, J. Zhang, C. Jiang, J. Huang, Z. Pang, Y. Cao, X. Wang, S. An, X. Wang, H. Huang, G. Yuan, Z. Yan, Degradation and osteogenic

induction of a $SrHPO_4$-coated Mg–Nd–Zn–Zr alloy intramedullary nail in a rat femoral shaft fracture model, Biomaterials 247 (2020) 119962.

[9] P.J. Marie, D. Felsenberg, M.L. Brandi, How strontium ranelate, via opposite effects on bone resorption and formation, prevents osteoporosis, Osteoporosis Int. 22 (2011) 1659–1667.

[10] E. Bonnelye, A. Chabadel, F. Saltel, P. Jurdic, Dual effect of strontium ranelate: stimulation of osteoblast differentiation and inhibition of osteoclast formation and resorption in vitro, Bone 42 (2008) 129–138.

[11] J.Y. Reginster, D. Felsenberg, S. Boonen, A. Diez-Perez, R. Rizzoli, M.L. Brandi, T.D. Spector, K. Brixen, S. Goemaere, C. Cormier, A. Balogh, P.D. Delmas, P.J. Meunier, Effects of long-term strontium ranelate treatment on the risk of nonvertebral and vertebral fractures in postmenopausal osteoporosis: results of a five-year, randomized, placebo-controlled trial, Arthritis Rheuma 58 (2008) 1687–1695.

[12] S. Tenti, S. Cheleschi, G.M. Guidelli, M. Galeazzi, A. Fioravanti, What about strontium ranelate in osteoarthritis? Doubts and securities, Mod. Rheumatol. 24 (2014) 881–884.

[13] E. Boanini, P. Torricelli, M. Gazzano, E. Della Bella, M. Fini, A. Bigi, Combined effect of strontium and zoledronate on hydroxyapatite structure and bone cell responses, Biomaterials 35 (2014) 5619–5626.

[14] E. Boanini, P. Torricelli, F. Sima, E. Axente, M. Fini, I.N. Mihailescu, A. Bigi, Strontium and zoledronate hydroxyapatites graded composite coatings for bone prostheses, J. Colloid Interface Sci. 448 (2015) 1–7.

[15] M. Schumacher, A. Henß, M. Rohnke, M.A. Gelinsky, Novel and easy-to-prepare Strontium(II) modified calcium phosphate bone cement with enhanced mechanical properties, Acta Biomater. 9 (2013) 7536–7544.

[16] A. Lode, C. Heiss, G. Knapp, J. Thomas, B. Nies, M. Gelinsky, M. Schumacher, Strontium-modified premixed calcium phosphate cements for the therapy of osteoporotic bone defects, Acta Biomater. 65 (2018) 475–485.

[17] M. Quade, M. Schumacher, A. Bernhardt, A. Lode, M. Kampschulte, A. Voß, P. Simon, O. Uckermann, M. Kirsch, M. Gelinsky, Strontium-modification of porous scaffolds from mineralized collagen for potential use in bone defect therapy, Mater. Sci. Eng. C-Mater. Biol. Appl. 84 (2018) 159–167.

[18] F. Salamanna, G. Giavaresi, D. Contartese, A. Bigi, E. Boanini, A. Parrilli, R. Lolli, A. Gasbarrini, G. Barbanti Brodano, M. Fini, Effect of strontium substituted ß-TCP associated to mesenchymal stem cells from bone marrow and adipose tissue on spinal fusion in healthy and ovariectomized rat, J. Cell Physiol. 234 (2019) 20046-20056.

[19] F. Salamanna, G. Giavaresi, A. Parrilli, P. Torricelli, E. Boanini, A. Bigi, M. Fini, Antiresorptive properties of strontium substituted and alendronate functionalized hydroxyapatite nanocrystals in an ovariectomized rat spinal arthrodesis model, Mater. Sci. Eng. C-Mater. Biol. Appl. 95 (2019) 355–362.

[20] M. Roy, G.A. Fielding, A. Bandyopadhyay, S. Bose, Effects of zinc and strontium substitution in tricalcium phosphate on osteoclast differentiation and resorption, Biomater. Sci. 1 (2013) 74–82.

[21] J. Chou, J. Hao, H. Hatoyama, B. Ben-Nissan, B. Milthorpe, M. Otsuka, The therapeutic effect on bone mineral formation from biomimetic zinc containing tricalcium phosphate (ZnTCP) in zinc-deficient osteoporotic mice, PLoS ONE 8 (2013) e71821

[22] E. Boanini, P. Torricelli, F. Sima, E. Axente, M. Fini, I.N. Mihailescu, A. Bigi, Gradient coatings of strontium hydroxyapatite/zinc β-tricalcium phosphate as a tool to modulate osteoblast/osteoclast response, J. Inorg. Biochem. 183 (2018) 1–8.

[23] M.P. Ginebra, C. Canal, M. Espanol, D. Pastorino, E.B. Montufar, Calcium phosphate cements as drug delivery materials, Adv. Drug. Deliv. Rev. 64 (2012) 1090–1110.

[24] A. Bigi, E. Boanini, Calcium phosphates as delivery systems for bisphosphonates, J. Funct. Biomater. 9 (2018) 6.

[25] A. Bigi, E. Boanini, C. Capuccini, M. Gazzano, Strontium-substituted hydroxyapatite nanocrystals, Inorg. Chim. Acta 360 (2007) 1009–1016.

[26] J. Terra, E.R. Dourado, J.G. Eon, D.E. Ellis, G. Gonzalez, A.M. Rossi, The structure of strontium-doped hydroxyapatite: an experimental and theoretical study, Phys. Chem. Chem. Phys. 11 (2009) 568–577.

[27] K. Matsunaga, H. Murata, Strontium substitution in bioactive calcium phosphates first-principles study, J. Phys. Chem. B 113 (2009) 3584–3589.

[28] G. Cheng, Y. Zhang, H. Yin, Y. Ruan, Y. Sun, K. Lin, Effects of strontium substitution on the structural distortion of hydroxyapatite by Rietveld refinement and Raman spectroscopy, Ceram. Int. 45 (2019) 11073–11078.

[29] A.A. Belik, F. Izumi, S.Y. Stefanovich, A.P. Malakho, B.I. Lazoryak, I.A. Leonidov, O.N. Leonidova, S.A. Davydov, Polar and centrosymmetric phases in solid solutions $Ca_{3-x}Sr_x(PO_4)_2$ ($0 \leq x \leq 16/7$), Chem. Mater. 14 (2002) 3197–3205.

[30] P. Nandha Kumar, M. Boovarasan, R.K. Singh, S. Kannan, Synthesis, structural analysis and fabrication of coatings of the Cu^{2+} and Sr^{2+} co-substitutions in β-$Ca_3(PO_4)_2$, RSC Adv. 3 (2013) 22469–22479.

[31] E. Boanini, M. Gazzano, C. Nervi, M.R. Chierotti, K. Rubini, R. Gobetto, A. Bigi, Strontium and zinc substitution in β-tricalcium phosphate: an X-ray diffraction, solid state NMR and ATR-FTIR study, J. Funct. Biomater. 10 (2019) 20.

[32] S.J. Saint-Jean, C.L. Camirè, P. Nevsten, S. Hansen, M.P. Ginebra, Study of the reactivity and in vitro bioactivity of Sr-substituted α-TCP cements, J. Mater. Sci. Mater. Med. 16 (2005) 993-1001.

[33] E. Boanini, M. Gazzano, K. Rubini, A. Bigi, Collapsed octacalcium phosphate stabilized by ionic substitutions, Cryst. Growth Des. 10 (2010) 3612–3617.

[34] H. Shi, T. Wu, J. Zhang, X. Ye, S. Zeng, X. Liu, T. Yu, J. Ye, C. Zhou, Biocompatible β-SrHPO4 clusters with dandelion-like structure as an alternative drug carrier, Mater. Sci. Eng. C-Mater. Biol. Appl. 81 (2017) 8–12.

[35] M. Sayahi, J. Santos, H. El-Feki, C. Charvillat, F. Bosc, I. Karacan, B. Milthorpe, C. Drouet, Brushite (Ca,M)HPO_4, $2H_2O$ doping with bioactive ions (M = Mg^{2+}, Sr^{2+}, Zn^{2+}, Cu^{2+}, and Ag^{+}): a new path to functional biomaterials? Mater. Today Chem. 16 (2020) 100230

[36] E. Boanini, F. Silingardi, M., Gazzano, A Bigi, Synthesis and hydrolysis of brushite (DCPD): the role of ionic substitution, Cryst. Growth Des. 21 (2021) 1689−1697.

[37] M. Catti, G. Ferraris, A. Filhol, Hydrogen bonding in the crystalline state. $CaHPO_4$ (Monetite), P-1 or PI? A novel neutron diffraction study, Acta Crystallogr. B 33 (1977) 1223-1229.

[38] M. Catti, G. Ferraris, S.A. Mason, Low-temperature ordering of hydrogen atoms in $CaHPO_4$ (monetite): X-ray and neutron diffraction study at 145 K, Acta Crystallogr. B 36 (1980) 254-259.

[39] B. Dickens, J.S. Bowen, W.E. Brown, A refinement of the crystal structure of $CaHPO_4$ (synthetic monetite), Acta Crystallogr. B 28 (1971) 797-806.

[40] L. Tortet, J.R. Gavarri, G. Nihoul, A.J. Dianoux, Study of protonic mobility in $CaHPO_4{\cdot}2H_2O$ (brushite) and $CaHPO_4$ (monetite) by infrared spectroscopy and neutron scattering, J. Solid State Chem. 132 (1997) 6–16.

[41] N. Ouerfelli, M.F. Zid, New polymorph of $CaHPO_4$ (monetite): synthesis and crystal structure, J. Struct. Chem. 57 (2016) 628-631.

[42] Z. Zou, X. Liu, L. Chen, K. Lin, J. Chang, Dental enamel-like hydroxyapatite transformed directly from monetite, J. Mater. Chem. 22 (2012) 22637-22641.

[43] S. Chen, M. Krumova, H. Cölfen, E.V. Sturm, Synthesis of fiber-like monetite without organic additives and its transformation to hydroxyapatite, Chem. Mater. 31 (2019) 1543–1551.

[44] B. Jokić, M. Mitrić, V. Radmilović, S. Drmanić, R. Petrović, D. Janaćković, Synthesis and characterization of monetite and hydroxyapatite whiskers obtained by a hydrothermal method, Ceram. Int. 37 (2011) 167–173.

[45] Y. Tokuoka, Y. Ito, K. Kitahara, Y. Niikura, A. Ochiai, N. Kawashima, Preparation of monetite ($CaHPO_4$) with hexagonally packed mesoporous structure by a sol–gel method using cationic surfactant aggregates as a template, Chem. Lett. 35 (2006) 1220–1221.

[46] M.G. Ma, Y.J. Zhu, J. Chang, Monetite formed in mixed solvents of water and ethylene glycol and its transformation to hydroxyapatite, J. Phys. Chem. B. 110 (2006) 14226–14230.

[47] A.C. Tas, Monetite ($CaHPO_4$) synthesis in ethanol at room temperature, J. Am. Ceram. Soc. 92 (2009) 2907–2912.

[48] F. Tamimi, J. Torres, D. Bassett, J. Barralet, E.L. Cabarcos, Resorption of monetite granules in alveolar bone defects in human patients, Biomaterials 31 (2010) 2762–2769.

[49] J. Zhang, W. Liu, V. Schnitzler, F. Tancret, J.M. Bouler, Calcium phosphate cements for bone substitution: chemistry, handling and mechanical properties, Acta Biomater. 10 (2014) 1035–1049.

[50] F. Tamimi, J. Torres, U. Gbureck, E.L. Cabarcos, D.C. Bassett, M.H. Alkhraisat, J.E. Barralet, Craniofacial vertical bone augmentation: a comparison between 3D printed monolithic monetite blocks and autologous onlay grafts in the rabbit, Biomaterials 30 (2009) 6318–6326.

[51] F. Tamimi, D.L. Nihouannen, H. Eimar, Z. Sheikh, S. Komarova, J. Barralet, The effect of autoclaving on the physical and biological properties of dicalcium phosphate dehydrate bioceramics: brushite vs. monetite, Acta Biomater. 8 (2012) 3161–3169.

[52] A. Oryan, S. Alidadi, A. Bigham-Sadegh, Dicalcium phosphate anhydrous: an appropriate bioceramic in regeneration of critical-sized radial bone defects in rats, Calcif. Tissue Int. 101 (2017) 530–544.

[53] X. Shi, C. Zhao, L. Xu, Q. Wang, Preparation of dicalcium phosphate anhydrous (monetite) biological coating on titanium by spray-drying method, Adv. Mater. Sci. Eng. (2017) Article ID 8281523, 7 pages

[54] L.B. Taher, L. Smiri, Y. Laligant, V. Maisonneuve, Investigation of the alkaline earth phosphates: synthesis and crystal structure of a new strontium hydrogen phosphate form, J. Solid State Chem. 152 (2000) 428-434.

[55] M. Roming, C. Feldmann, Selective synthesis of α- and β-$SrHPO_4$ nanoparticles, J. Mater. Sci. 43 (2008) 5504–5507.

[56] F.Q. Zhuang, R.Q. Tan, W.F. Shen, X.P. Zhang, W. Xu, W.J. Song, Synthesis of β-type strontium hydrogen phosphate nanosheets and its immobilization of Pb^{2+} in acidic aqueous solution, Acta Metall. Sin. (Engl. Lett.) 28 (2015) 438–443.

[57] Z. Lu, W. Chu, R. Tan, S. Tang, F. Xu, W. Song, J. Zhao, Facile synthesis of β-$SrHPO_4$ with wide applications in the effective removal of Pb^{2+} and methyl blue, J. Chem. Eng. Data 62 (2017) 3501−3511.

[58] L. Forte, P. Torricelli, E. Boanini, M. Gazzano, K. Rubini, M. Fini, A. Bigi, Antioxidant and bone repair properties of quercetin functionalized hydroxyapatite: an in vitro osteoblast–osteoclast– endothelial cell co-culture study, Acta Biomater. 32 (2016) 298–308.

[59] B. Jokić, M. Mitrić, V. Radmilović, S. Drmanić, R. Petrović, D. Janaćković, Synthesis and characterization of monetite and hydroxyapatite whiskers obtained by a hydrothermal method, Ceram. Int. 37 (2011) 167–173.

[60] A. Boudjada, R. Masse, J.C. Guttel, Structure cristalline de l'orthophosphate monoacide de strontium: $SrHPO_4$ α: forme triclinique, Acta Crystallogr. B 34 (1978) 2692-2695.

[61] R.A. Young, The Rietveld Method, Oxford University Press, Oxford, 1993.

[62] J. Xu, I.S. Butler, D.F.R. Gilson, FT-Raman and high-pressure infrared spectroscopic studies of dicalcium phosphate dihydrate ($CaHPO_4·2H_2O$) and anhydrous dicalcium phosphate ($CaHPO_4$), Spectrochim. Acta A 55 (1999) 2801–2809.

[63] B. Louati, K. Guidara, M. Gargouri, M. Fourati, ^{1}H NMR, ^{31}P NMR and Raman Study of $CaHPO_4$ and $SrHPO_4$, Z. Naturforsch. 60a (2005) 121–126.

[64] K. Rubini, E. Boanini, A. Bigi, Role of aspartic and polyaspartic acid on the synthesis and hydrolysis of brushite, J. Funct. Biomater. 10 (2019) 11 (12 pages).

Captions to the figures

Figure 1 - Monetite, $CaHPO_4$, triclinic α-form. a) polyhedral assembly view down *b*-axis; b) and c) cation environment, green: Sr1 site, yellowish: Sr2 site.

Figure 2. (a) XRD patterns of samples obtained by direct synthesis; (b) expansion of the 12°-24° range showing that peaks undergo 2θ shift and variations in the diffraction intensities.

Figure 3. (a) Rietveld plot for refinement of DS-80; (b) plot of cell parameters for DS samples on varying Sr content.

Figure 4. (a) FTIR-ATR spectra and (b) SEM images of DS samples.

Figure 5. (a) DSC curves of the DCPD samples synthesized at increasing Sr content; (b) XRD plots and (c) SEM images of TT samples obtained after thermal treatment (Scale bar=20μm in all images).

Figure 6. (a) XRD patterns and (b) SEM images of samples obtained at low temperature. In (a) the reference lines of β-$SrHPO_4$ (ICDD file 12-368) and DCPD (ICDD file 9-077) are reported. Symbols in β-60 indicate the presence of (*) β-$SrHPO_4$ and (○) α-$Sr_2P_2O_7$.

Figure 7. (a) Rietveld plot for β-$SrHPO_4$: refinement fit (blue line) against experimental data (red dots). Differential plot (gray line) between observed and calculated intensity. Blue vertical sticks represent the angular positions of the expected *hkl* reflections. (b) and (c) Views of β-$SrHPO_4$ crystal structure down *c*-axis; and (c) environments of Sr atoms.

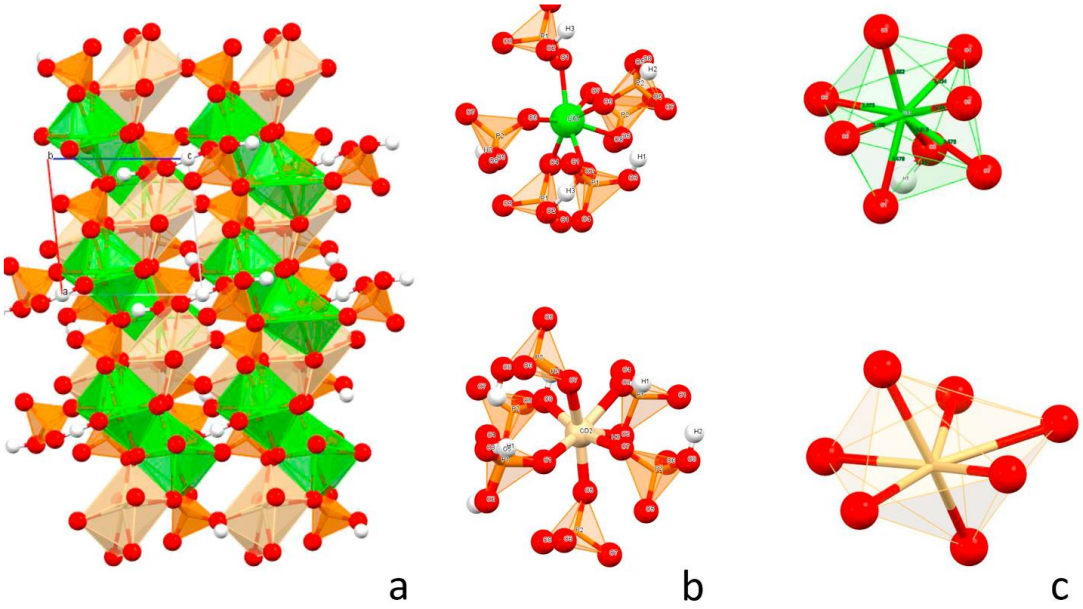

Figure 1

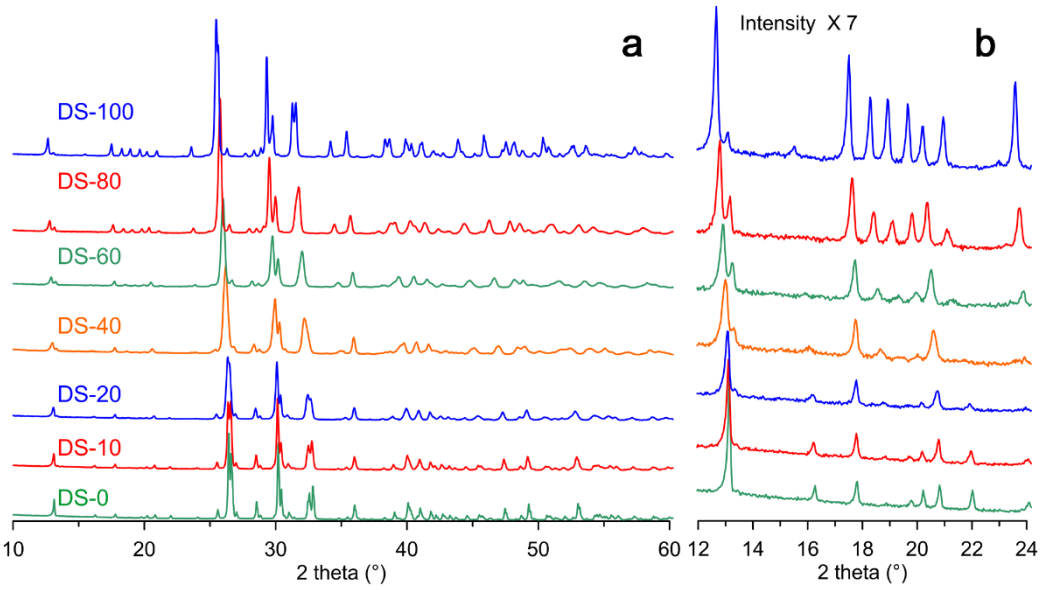

Figure 2

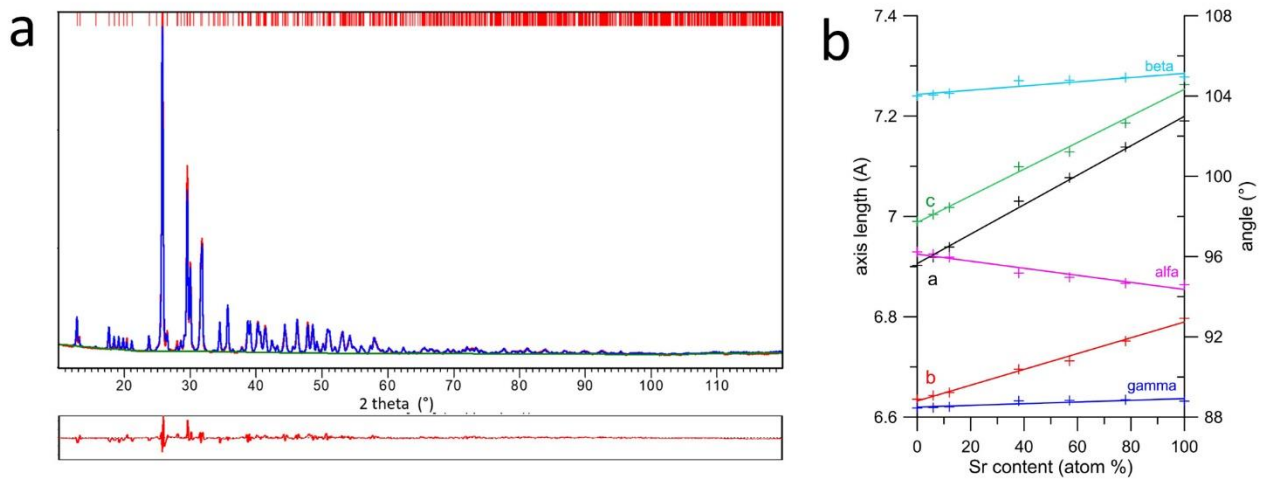

Figure 3

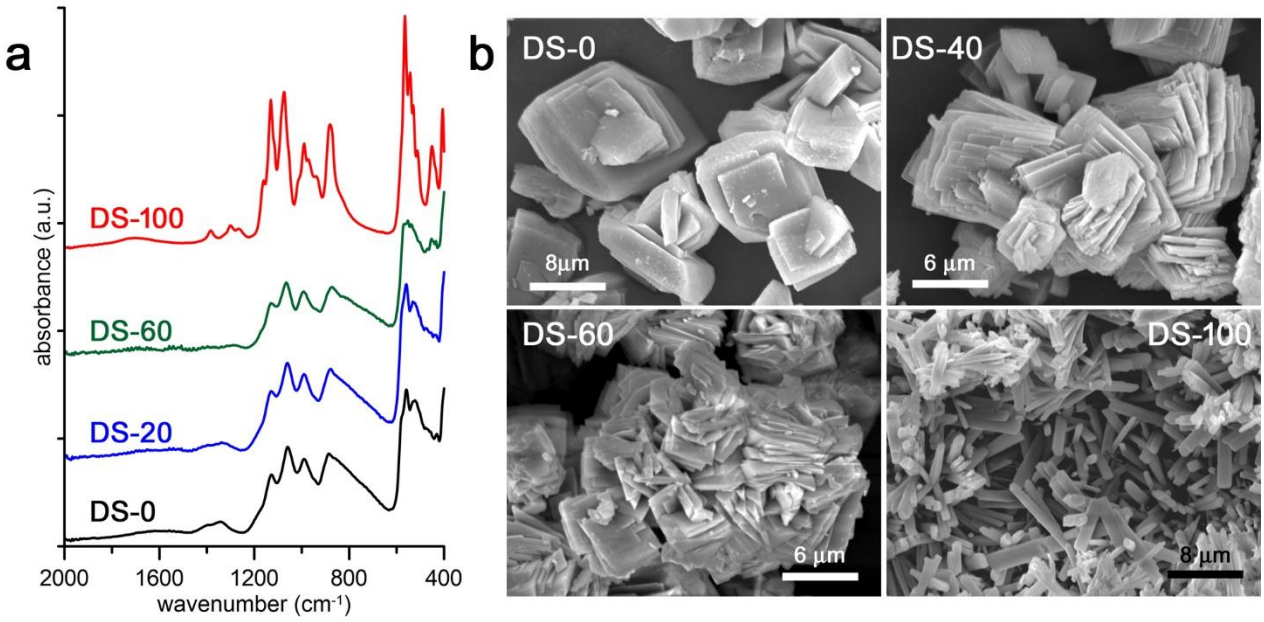

Figure 4

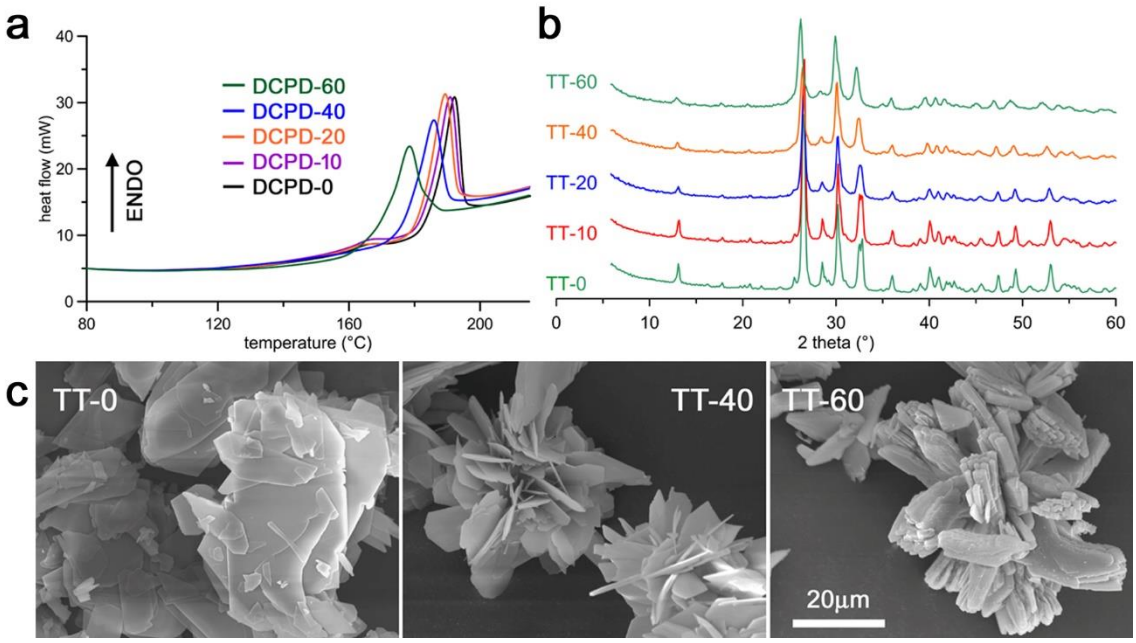

Figure 5

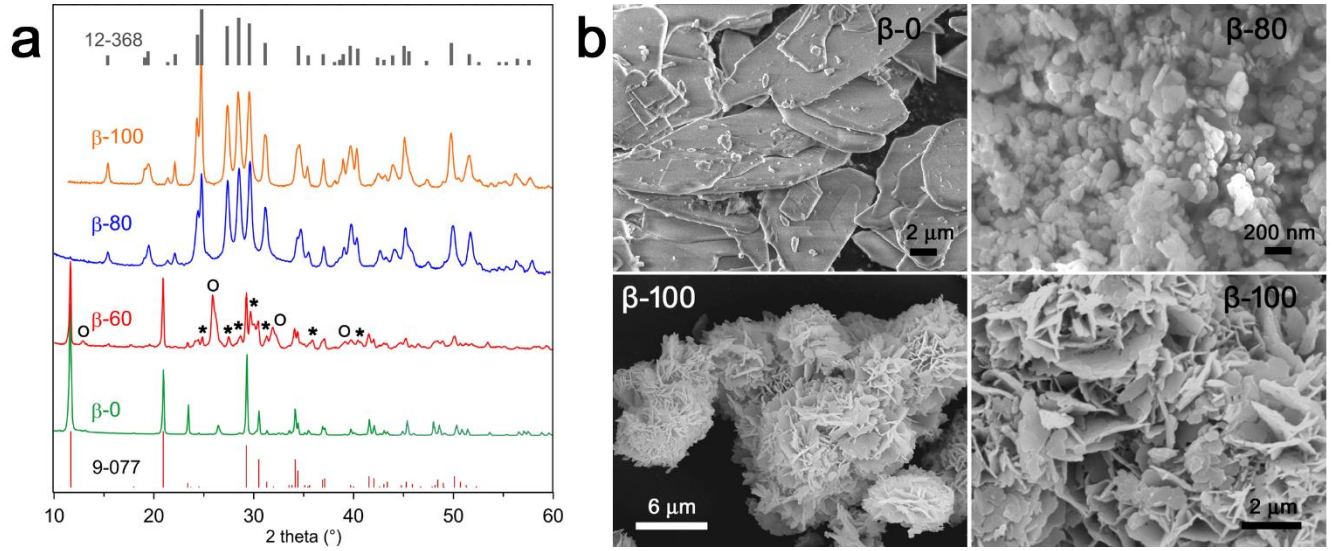

Figure 6

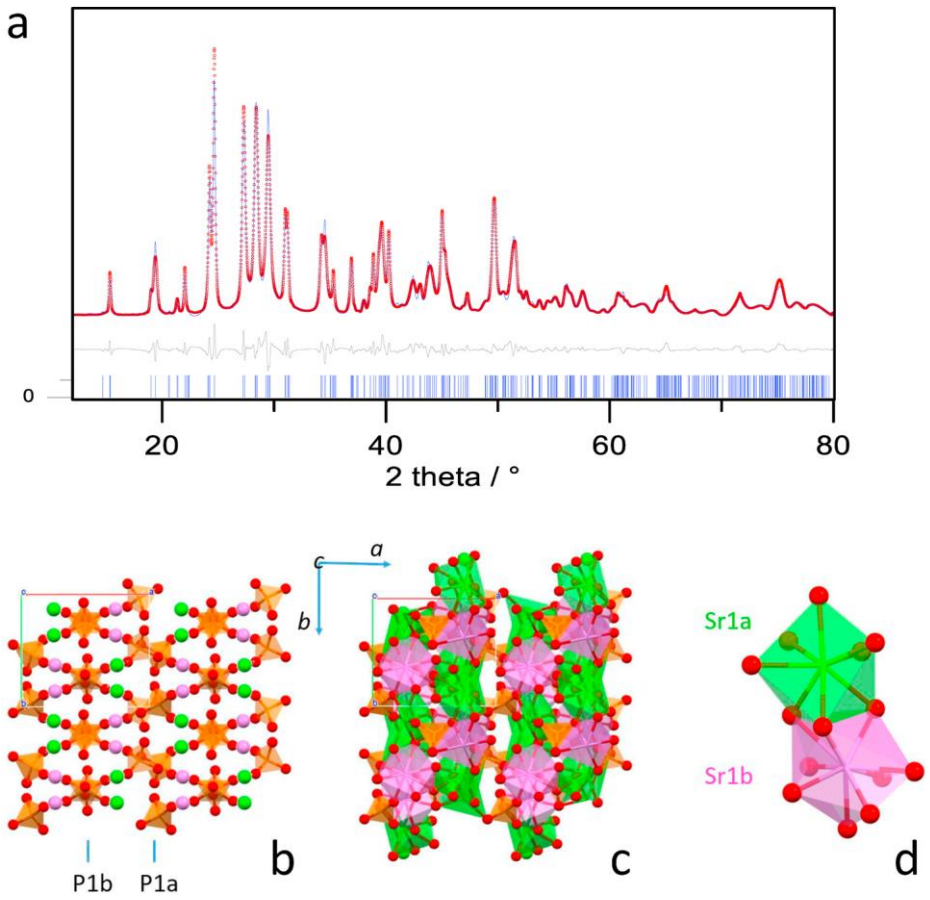

Figure 7